RESEARCH DEPARTMENT REPORT SERIES no. 81-2011 ISSN 1749-8775

SEABED PREHISTORY AREA 240
OPTICAL DATING OF SUBMARINE CORES

SCIENTIFIC DATING REPORT

Phil Toms

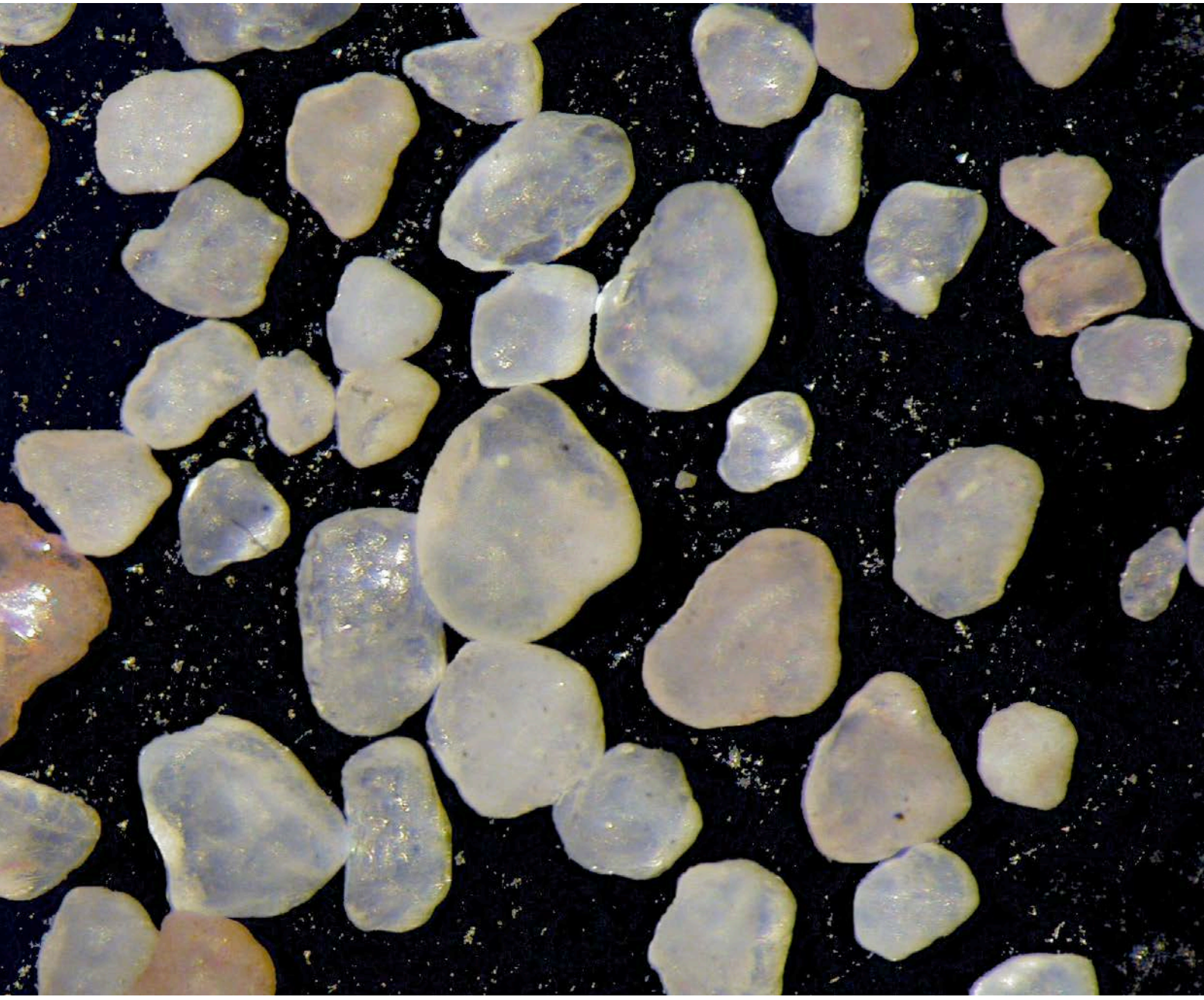

ARCHAEOLOGICAL SCIENCE

ENGLISH HERITAGE

Research Department Report Series 81-2011

SEABED PREHISTORY AREA 240

OPTICAL DATING OF SUBMARINE CORES

Phil Toms

Grid ref: 663883 303893

© English Heritage

ISSN 1749-8775

The Research Department Report Series incorporates reports from all the specialist teams within the English Heritage Research Department: Archaeological Science; Archaeological Archives; Historic Interiors Research and Conservation; Archaeological Projects; Aerial Survey and Investigation; Archaeological Survey and Investigation; Architectural Investigation; Imaging, Graphics and Survey, and the Survey of London. It replaces the former Centre for Archaeology Reports Series, the Archaeological Investigation Report Series and the Architectural Investigation Report Series.
Many of these are interim reports which make available the results of specialist investigations in advance of full publication. They are not usually subject to external refereeing, and their conclusions may sometimes have to be modified in the light of information not available at the time of the investigation. Where no final project report is available, readers must consult the author before citing these reports in any publication. Opinions expressed in Research Department reports are those of the author(s) and are not necessarily those of English Heritage.

Requests for further hard copies, after the initial print run, can be made by emailing:
Res.reports@english-heritage.org.uk
or by writing to:
English Heritage, Fort Cumberland, Fort Cumberland Road, Eastney, Portsmouth PO4 9LD
Please note that a charge will be made to cover printing and postage.

SUMMARY

This study contributes to the Seabed Prehistory Area 240 project, providing Optical age estimates for nine sediment samples obtained from four vibrocores. The time-dependent optically stimulated luminescence signal was calibrated from multi-grain, fine sand aliquots using a single-aliquot, regenerative-dose protocol to provide a measure of natural dose absorption during the burial period. This dosimetry was converted into chronometry by assessing the rate of dose absorption, accounting for litho-cosmogenic emissions along with moisture absorption and grain size attenuation effects. The Optical age estimates generated in this study span from 31 ka (Marine Isotope Stage 2) to greater than 869 ka (Marine Isotope Stage 24). The majority of samples are accompanied by analytical caveats, however all intra-core age estimates are consistent with their relative stratigraphic position. Dose rates are below average for most samples; in such cases age estimates become increasingly sensitive to inaccuracies in D_r as the magnitude of D_r decreases and burial period increases. The reliability of the optical chronology should be measured against any extrinsic temporal control that may be available to the project. If units dated in this study can be shown to be stratigraphically equivalent between cores then it may be possible to assess reliability intrinsically, quantifying the convergence of age estimates from divergent D_r values.

CONTRIBUTORS

Dr Phil Toms (University of Gloucestershire) and Jack Russell (Wessex Archaeology)

ACKNOWLEDGEMENTS

The OSL dating formed a part of the Seabed Prehistory Project, which is under the direction of Antony Firth (Wessex Archaeology) and funded by English Heritage through the Aggregates Levy Sustainability Fund.

ARCHIVE LOCATION

Wessex Archaeology, Portway House, Old Sarum Park, Salisbury, SP4 6EB

DATE OF INVESTIGATION

2010

CONTACT DETAILS

Geochronology Laboratories, School of Natural and Social Sciences, University of Gloucestershire, Swindon Road, Cheltenham GL50 4AZ. Tel: 01242 714708
Email: ptoms@glos.ac.uk

CONTENTS

1.0 Introduction 1
2.0 Optical Dating: Mechanisms and Principles 3
3.0 Sample Collection and Preparation 3
4.0 Acquisition and Accuracy of D_e Value 4
4.1 Laboratory factors 5
4.1.1 Feldspar contamination 5
4.1.2 Preheating 5
4.1.3 Irradiation 6
4.1.4 Internal consistency 7
4.2 Environmental factors 7
4.2.1 Incomplete zeroing 7
4.2.2 Turbation 8
5.0 Acquisition and Accuracy of D_r Value 8
6.0 Estimation of Age 9
7.0 Analytical Uncertainty 9
8.0 Summary and Recommendations 10
9.0 References 12
Tables 15
Appendix 1: Technical Data for Sample GL10038 17
Appendix 2: Technical Data for Sample GL10039 18
Appendix 3: Technical Data for Sample GL10040 19
Appendix 4: Technical Data for Sample GL10041 20
Appendix 5: Technical Data for Sample GL10037 21
Appendix 6: Technical Data for Sample GL10042 22
Appendix 7: Technical Data for Sample GL10045 23
Appendix 8: Technical Data for Sample GL10044 24
Appendix 9: Technical Data for Sample GL10043 25

1.0 INTRODUCTION

The southern North Sea is an area well known for its prehistoric remains and complex sedimentary sequences. Whilst Pleistocene megafaunal remains have been recovered from the southern North Sea for many years, in 2008 a large group of Palaeolithic stone artefacts were recovered from Area 240, an aggregate extraction area 11km east of Great Yarmouth. These artefacts were discovered at SBV Flushing Wharf, near Antwerp by Mr Jan Meulmeester and are thought to derive from a discrete 3.5 x 1.1km area within Area 240. This area has been subject to a voluntary exclusion zone put in place by Hanson Aggregates Marine Ltd since the discovery of the artefacts.

In response to these significant discoveries within the area, Wessex Archaeology further developed the Seabed Prehistory project, supported by a grant from the Aggregate Levy Sustainability Fund administered by English Heritage in order to further investigate the deposits from the area where the artefacts are thought to have derived. The project included a review of existing geophysical and geotechnical data, followed by a programme of targeted geophysical and geotechnical survey. The geotechnical survey included targeting palaeogeographic features identified within the geophysical data and areas where artefacts were recovered using clamshell grabs and benthic trawls. These data were integrated to further inform a borehole survey undertaken in May 2010 using a 6 metre high powered vibrocore unit deployed from the Fugro Ltd survey vessel *VOS Baltic*. A total of ten vibrocore locations was chosen within Area 240 and at each location two vibrocores were retrieved, one of which was recovered in an opaque liner specifically for Optical dating.

The aim of the Optical dating was to secure the chronological framework for the sedimentary sequence of Pleistocene sands and gravels from which the artefactual remains were dredged. A total of nine samples from four vibrocores (VC2b, VC3b, VC7b, and VC9b) were submitted for Optical dating (Fig 1).

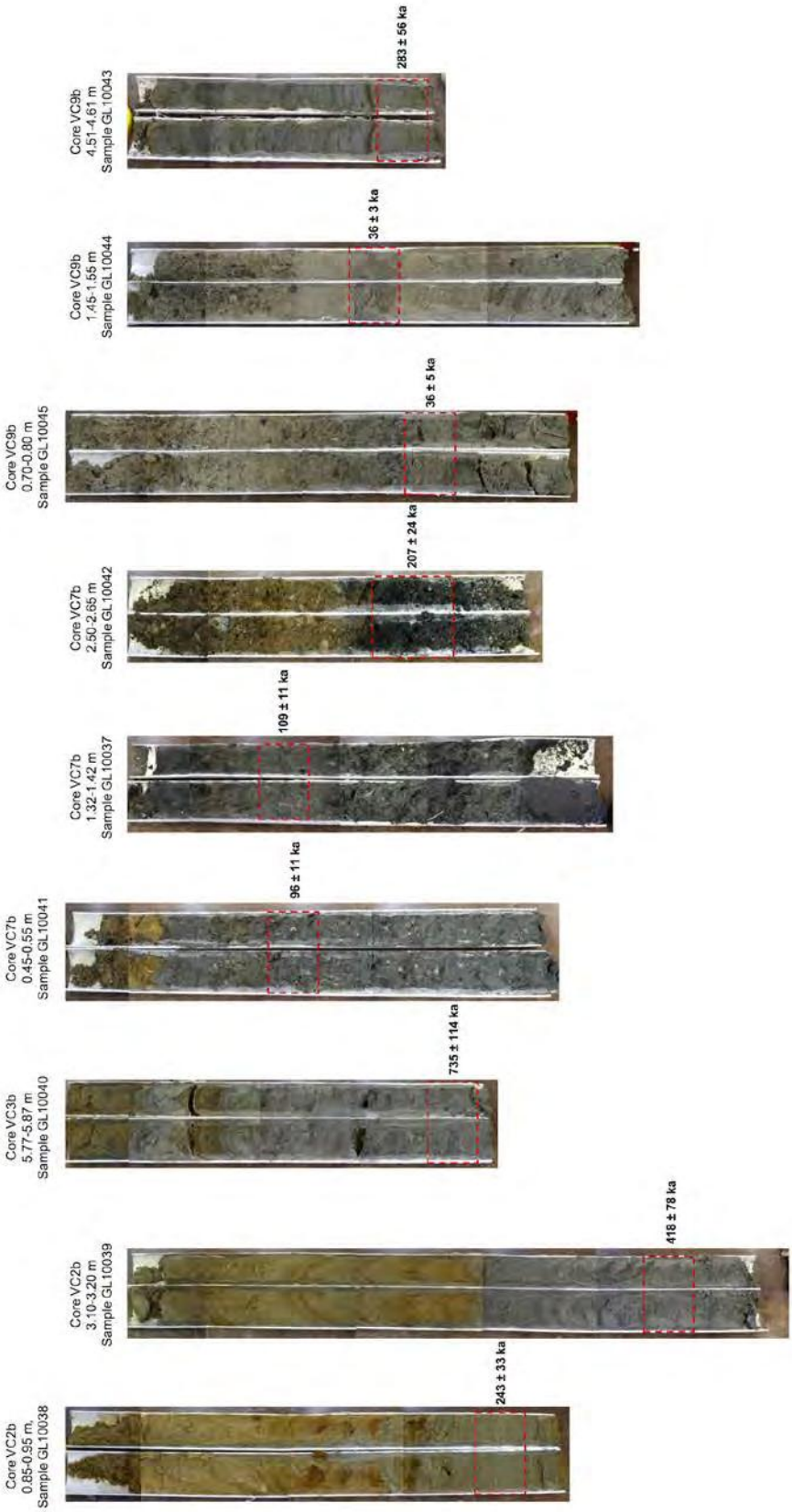

Figure 1. Cores, sample positions and associated optical age estimate

2.0 OPTICAL DATING: MECHANISMS AND PRINCIPLES

Upon exposure to ionising radiation, electrons within the crystal lattice of insulating minerals are displaced from their atomic orbits. Whilst this dislocation is momentary for most electrons, a portion of charge is redistributed to meta-stable sites (traps) within the crystal lattice. In the absence of significant optical and thermal stimuli, this charge can be stored for extensive periods. The quantity of charge relocation and storage relates to the magnitude and period of irradiation. When the lattice is optically or thermally stimulated, charge is evicted from traps and may return to a vacant orbit position (hole). Upon recombination with a hole, an electron's energy can be dissipated in the form of light-generating crystal luminescence, providing a measure of dose absorption.

Herein, quartz is segregated for dating. The utility of this minerogenic dosimeter lies in the stability of its datable signal over the mid to late Quaternary period, predicted through isothermal decay studies (eg Smith *et al* 1990; retention lifetime 630Ma at 20°C) and evidenced by optical age estimates concordant with independent chronological controls (eg Murray and Olley 2002). This stability is in contrast to the anomalous fading of comparable signals commonly observed for other ubiquitous sedimentary minerals, such as feldspar and zircon (Wintle 1973; Templer 1985; Spooner 1993).

Optical age estimates of sedimentation (Huntley *et al* 1985) are premised upon reduction of the minerogenic time-dependent signal (Optically Stimulated Luminescence, OSL) to zero through exposure to sunlight and, once buried, signal reformulation by absorption of litho- and cosmogenic radiation. The signal accumulated post-burial acts as a dosimeter recording total dose absorption, converting to a chronometer by estimating the rate of dose absorption quantified through the assay of radioactivity in the surrounding lithology and streaming from the cosmos.

$$\text{Age} = \text{Mean Equivalent Dose } (D_e, \text{Gy}) / \text{Mean Dose Rate } (D_r, \text{Gy.ka}^{-1})$$

Aitken (1998), Bøtter-Jensen *et al* (2003) and Duller (2008) offer a detailed review of optical dating.

3.0 SAMPLE COLLECTION AND PREPARATION

A total of nine sediment samples were submitted from four vibrocores for Optical dating (Table 1; Fig 1). The cores were bisected in daylight to identify the apposite sampling position in consultation with J Russell, Wessex Archaeology, to meet the requirements of the client. To preclude optical erosion of the datable signal prior to measurement both lengths of each core were moved into, and prepared under, controlled laboratory illumination, provided by Encapsulite RB-10 (red) filters. Sediment exposed to daylight during bisection was removed from each sample position to a depth of 10 mm from each bisected face. The remaining sediment was then sectioned into a 100 mm length, 40 mm wide sample using aluminium separators to preclude incorporation of material transferred down the core walls during submarine retrieval. In the case of sample GL10042, a length

of 150 mm was extracted in order to attain sufficient fine sand in the predominantly coarse sand matrix. Sub-samples of *c* 50 g were taken from within each position to establish β D_r values and, where feasible, further samples beyond each sample position were taken to estimate γ D_r values.

Each dating sample was then weighed, dried, reweighed, and sieved. Quartz within the fine sand (125–180, 180–250 μm) fraction was segregated (Table 1). The samples were then subjected to acid and alkaline digestion (10% HCl, 15% H_2O_2) to attain removal of carbonate and organic components respectively. A further acid digestion in HF (40%, 60 mins) was used to etch the outer 10–15 μm layer affected by α radiation and degrade each samples' feldspar content. During HF treatment, continuous magnetic stirring was used to effect isotropic etching of grains. 10% HCl was then added to remove acid soluble fluorides. Each sample was dried, resieved, and quartz isolated from the remaining heavy mineral fraction using a sodium polytungstate density separation at 2.68g.cm^{-3}. Twelve multi-grain aliquots (*c* 4–6 mg) of quartz from each sample were then mounted on aluminium discs for determination of D_e values.

All drying was conducted at 40°C to prevent thermal erosion of the time-dependent signal. All acids and alkalis were Analar grade. All dilutions (removing toxic-corrosive and non-minerogenic luminescence-bearing substances) were conducted with distilled water to prevent signal contamination by extraneous particles.

4.0 ACQUISITION AND ACCURACY OF D_E VALUE

All minerals naturally exhibit marked inter-sample variability in luminescence per unit dose (sensitivity). Therefore, the estimation of D_e acquired since burial requires calibration of the natural signal using known amounts of laboratory dose. D_e values were quantified using a single-aliquot regenerative-dose (SAR) protocol (Murray and Wintle 2000; 2003) facilitated by a Risø TL-DA-15 irradiation-stimulation-detection system (Markey *et al*., 1997; Bøtter-Jensen *et al* 1999). Within this apparatus, optical signal stimulation is provided by a 150 W tungsten halogen lamp, filtered to a broad blue-green light, 420-560 nm (2.21-2.95 eV) conveying 16 mWcm^{-2}, using three 2 mm Schott GG420 and a broadband interference filter. Infrared (IR) stimulation, provided by 6 IR diodes (Telefunken TSHA 6203) stimulating at 875±80nm delivering ~5 mW.cm^{-2}, was used to indicate the presence of contaminant feldspars (Hütt *et al* 1988). Stimulated photon emissions from quartz aliquots are in the ultraviolet (UV) range and were filtered from stimulating photons by 7.5 mm HOYA U-340 glass and detected by an EMI 9235QA photomultiplier fitted with a blue-green sensitive bialkali photocathode. Aliquot irradiation was conducted using a 1.48 GBq ^{90}Sr/^{90}Y β source calibrated for multi-grain aliquots of fine sand sized quartz against the 'Hotspot 800' ^{60}Co γ source located at the National Physical Laboratory (NPL), UK.

SAR by definition evaluates D_e through measuring the natural signal (Fig 1 in each Appendix) of a single aliquot and then regenerating that aliquot's signal by using known laboratory doses to enable calibration. For each aliquot, 5 different regenerative-doses were administered so as to image dose response. D_e values for each aliquot were then interpolated, and associated counting and fitting errors calculated, by way of exponential plus linear regression (Fig 1 in each Appendix). Weighted (geometric) mean D_e values were calculated from 12 aliquots using the central age model outlined by Galbraith *et al* (1999) and are quoted at 1σ confidence. The accuracy with which D_e equates to total absorbed dose and that dose absorbed since burial was assessed. The former can be considered a function of laboratory factors, the latter, one of environmental issues. Diagnostics were deployed to estimate the influence of these factors and criteria instituted to optimise the accuracy of D_e values.

4.1 Laboratory factors

4.1.1 Feldspar contamination

The propensity of feldspar signals to fade and underestimate age, coupled with their higher sensitivity relative to quartz, makes it imperative to qualify feldspar contamination. At room temperature, feldspars generate a signal (IRSL) upon exposure to IR, whereas quartz does not. The signal from feldspars contributing to OSL can be depleted by prior exposure to IR. For all aliquots the contribution of any remaining feldspars was estimated from the OSL IR depletion ratio (Duller 2003). If the addition to OSL by feldspars is insignificant, then the repeat dose ratio of OSL to post-IR OSL should be statistically consistent with unity (Figs 1 and 5 in each Appendix). If any aliquots do not fulfil this criterion, as in the case of GL10042 and GL10043, then the sample age estimate should be accepted tentatively. Any aliquots that did not fulfil this criterion were rejected. The source of feldspar contamination is rarely rooted in sample preparation; it predominantly results from the occurrence of feldspars as inclusions within quartz.

4.1.2 Preheating

Preheating aliquots between irradiation and optical stimulation is necessary to ensure comparability between natural and laboratory-induced signals. However, the multiple irradiation and preheating steps that are required to define single-aliquot regenerative-dose response leads to signal sensitisation, rendering calibration of the natural signal inaccurate. The SAR protocol (Murray and Wintle, 2000; 2003) enables this sensitisation to be monitored and corrected using a test dose, here set at 10 Gy preheated to 220°C for 10s, to track signal sensitivity between irradiation-preheat steps. However, the accuracy of sensitisation correction for both natural and laboratory signals can be preheat dependent.

The Dose Recovery test was used to assess the optimal preheat temperature for accurate correction and calibration of the time dependent signal. Dose Recovery (Fig 2 in each Appendix) attempts to quantify the combined effects of thermal transfer and sensitisation on the natural signal, using a precise lab dose to simulate natural dose. The ratio between the applied dose and recovered D_e value should be statistically concordant with unity. For this diagnostic, 6 aliquots were each assigned a 10 s preheat between 180°C and 280°C.

That preheat treatment fulfilling the criterion of accuracy within the Dose Recovery test (Table 1) was selected to generate the final D_e value. Two samples, GL10041 and GL10043, failed to retrieve the applied dose irrespective of preheat treatment; their associated age estimates should therefore be accepted tentatively. Further thermal treatments, prescribed by Murray and Wintle (2000; 2003), were applied to optimise accuracy and precision. Optical stimulation was conducted at 125°C in order to minimise effects associated with photo-transferred thermoluminescence and maximise signal to noise ratios. Inter-cycle optical stimulation was conducted at 280°C to minimise recuperation.

4.1.3 Irradiation

For all samples having D_e values in excess of 100 Gy, matters of signal saturation and laboratory irradiation effects are of concern. With regards the former, the rate of signal accumulation generally adheres to a saturating exponential form and it is this that limits the precision and accuracy of D_e values for samples having absorbed large doses. For such samples, the functional range of D_e interpolation by SAR has been verified up to 600 Gy by Pawley *et al* (2010). Age estimates based on D_e values exceeding this value should be accepted tentatively. Whilst no mean D_e value exceeded 600 Gy, 25% of aliquots in GL10040 did with the natural dose proving to be saturated. In this case, the resulting age estimate is considered a minimum value.

4.1.4 Internal consistency

Quasi-radial plots (Fig 5 in each Appendix; cf Galbraith 1990) are used to illustrate inter-aliquot D_e variability for natural, repeat regenerative-dose and OSL to post-IR OSL signals (Figs 3 to 5, respectively, in each Appendix). D_e values are standardised relative to the central D_e value for natural signals and applied dose for regenerated signals. D_e values are described as overdispersed when >5% lie beyond $\pm 2\sigma$ of the standardising value; resulting from a heterogeneous absorption of burial dose and/or response to the SAR protocol. For multi-grain aliquots, overdispersion of natural signals does not necessarily imply inaccuracy. However where overdispersion is observed for regenerated signals, as in the case of all but one sample (GL10037) in this study, the resulting age estimate should be accepted tentatively.

4.2 Environmental factors

4.2.1 Incomplete zeroing

Post-burial OSL signals residual of pre-burial dose absorption can result where pre-burial sunlight exposure is limited in spectrum, intensity and/or period, leading to age overestimation. This effect is particularly acute for material eroded and redeposited sub-aqueously (Olley *et al* 1998; 1999; Wallinga 2002) and exposed to a burial dose of <20 Gy (eg Olley *et al* 2004). It has some influence in sub-aerial contexts but is rarely of consequence where aerial transport has occurred.

Within single-aliquot regenerative-dose optical dating there are two diagnostics of partial resetting (or bleaching); signal analysis (Agersnap-Larsen *et al* 2000; Bailey *et al* 2003) and inter-aliquot D_e distribution studies (Murray *et al* 1995). Within this study, signal analysis was used to quantify the change in D_e value with respect to optical stimulation time for multi-grain aliquots. This exploits the existence of traps within minerogenic dosimeters that bleach with different efficiency for a given wavelength of light to verify partial bleaching. $D_e(t)$ plots (Fig 6 in each Appendix; Bailey *et al* 2003) are constructed from separate integrals of signal decay as laboratory optical stimulation progresses. A statistically significant increase in natural $D_e(t)$ is indicative of partial bleaching assuming three conditions are fulfilled. Firstly, that a statistically significant increase in $D_e(t)$ is observed when partial bleaching is simulated within the laboratory. Secondly, that there is no significant rise in $D_e(t)$ when full bleaching is simulated. Finally, there should be no significant augmentation in $D_e(t)$ when zero dose is simulated. Where partial bleaching is detected, as in the case of sample GL10042, the age derived from the sample should be considered a maximum estimate only. However, the utility of signal analysis is strongly dependent upon a samples pre-burial experience of sunlight's spectrum and its residual to post-burial signal ratio. Given in the majority of cases, the spectral exposure history of a deposit is uncertain, the absence of an increase in natural $D_e(t)$ does not necessarily testify to the absence of partial bleaching.

4.2.2 Turbation

The accuracy of sedimentation ages can further be controlled by post-burial trans-strata grain movements forced by pedo- or cryoturbation (eg Bateman *et al* 2003). Though assumed to reflect former terrestrial sediments, none of the samples showed visible signs of pedogenesis or cryogenic deformation.

5.0 ACQUISITION AND ACCURACY OF D_R VALUE

Lithogenic D_r values were defined through measurement of U, Th and K radionuclide concentration and conversion of these quantities into β and γ D_r values external to the quartz grains (Table 1). External β contributions were estimated from sub-samples by laboratory-based γ spectrometry using an Ortec GEM-S high purity Ge coaxial detector system, calibrated using certified reference materials supplied by CANMET. γ dose rates can be estimated from *in situ* NaI gamma spectrometry to reduce uncertainty relating to potential heterogeneity in the γ dose field surrounding each sample. Where direct measurements are unavailable as in the present case, laboratory-based Ge γ spectrometry can be used to profile the γ field. Where feasible, sub-samples at intervals within 300 mm above and below of each sample's centre were taken, individually homogenised and then combined in proportion to the γ gradient hypothesised by Løvborg (Aitken 1985). Estimates of radionuclide concentration were converted into D_r values (Adamiec and Aitken 1998), accounting for D_r modulation forced by grain size (Mejdahl 1979) and present moisture content (Zimmerman 1971). Internal α D_r was assumed to be 0.06 ± 0.03 $Gy.ka^{-1}$. Cosmogenic D_r values were calculated on the basis of sample depth, geographical position and matrix density (Prescott and Hutton 1994).

The spatiotemporal validity of D_r values can be considered a function of five variables. Firstly, age estimates devoid of *in situ* γ spectrometry data or laboratory-based γ profiling should be accepted tentatively; this applies to samples GL10038, GL10040 and GL10043. Secondly, disequilibrium can force temporal instability in U and Th emissions (Olley *et al* 1996). Though considered prevalent in surficial marine sediments, owing principally to unsupported U isotopes scavenged from the water column (Jakobsen *et al* 2003; Stokes *et al* 2003), the assumed terrestrial genus of the deposits should mean that significant disequilibrium is unlikely. However, samples GL10038 and possibly GL10043 show this effect to be pronounced (>50% disequilibrium between ^{238}U and ^{226}Ra; Fig 7 in each Appendix) and thus the resulting age estimates should be accepted tentatively. It may be that U disequilibrium is relatively significant in other samples, but the low concentration of this radionuclide in most of the samples precludes precise detection. Thirdly, variations in matrix composition forced by pedogenesis or cryoturbation, such as radionuclide and/or mineral remobilisation, may alter the rate of energy emission and/or absorption. However, no turbation was apparent within this study's samples. Fourthly, spatiotemporal detractions from present moisture content are difficult to assess directly, requiring knowledge of the magnitude and timing of differing contents. There is also the possibility

in the present study that prior to measurement, moisture content may have reduced during storage; to counter this a 50% uncertainty has been attached to measured moisture content. The maximum influence of moisture content variations can be delimited by recalculating D_r for minimum (zero) and maximum (saturation; 40±5% for sand matrices) content. Finally, temporal alteration in the thickness of overburden alters cosmic D_r values. Cosmic D_r often forms a negligible portion of total D_r, but in the present case constitutes up to 31%. It is possible to quantify the maximum influence of overburden flux by recalculating D_r for minimum (zero) and maximum (surface sample) cosmic D_r.

6.0 ESTIMATION OF AGE

Age estimates reported in Table 1 provide an estimate of sediment burial period based on mean D_e and D_r values and their associated analytical uncertainties. Uncertainty in age estimates is reported as a product of systematic and experimental errors, with the magnitude of experimental errors alone shown in parentheses (Table 1). Probability distributions indicate the inter-aliquot variability in age (Fig 8 in each Appendix). The maximum influence of temporal variations in D_r forced by minima-maxima variation in moisture content and overburden thickness is illustrated in Figure 8 in each Appendix. Where uncertainty in these parameters exists, this age range may prove instructive, but the combined extremes represented should not be construed as preferred age estimates.

7.0 ANALYTICAL UNCERTAINTY

All errors are based upon analytical uncertainty and quoted at 1σ confidence. Error calculations account for the propagation of systematic and/or experimental (random) errors associated with D_e and D_r values.

For D_e values, systematic errors are confined to laboratory β source calibration. Uncertainty in this respect is that combined from the delivery of the calibrating γ dose (1.2%; NPL pers comm), the conversion of this dose for SiO_2 using the respective mass energy-absorption coefficient (2%; Hubbell 1982) and experimental error, totalling 3.5%. Mass attenuation and Bremsstrahlung losses during γ dose delivery are considered negligible. Experimental errors relate to D_e interpolation using sensitisation-corrected dose responses. Natural and regenerated sensitisation corrected dose points (S_i) are quantified by

$$S_i = (D_i - x.L_i) / (d_i - x.L_i) \qquad \text{Eq 1}$$

where D_i = Natural or regenerated OSL, initial 0.2s

L_i = Background natural or regenerated OSL, final 5s

d_i = Test dose OSL, initial 0.2s

x = Scaling factor, 0.08

The error on each signal parameter is based on counting statistics, reflected by the square-root of measured values. The propagation of these errors within Eq 1 generating σS_i follows the general formula given in Eq 2. σS_i are then used to define fitting and interpolation errors within linear or exponential regressions (Green and Margerison 1978; Ixaru and Vanden Berghe 2004).

For D_r values, systematic errors accommodate uncertainty in radionuclide conversion factors (5%), β attenuation coefficients (5%), a-value (4%; derived from a systematic α source uncertainty of 3.5% and experimental error), matrix density (0.20 $g.cm^{-3}$), vertical thickness of sampled section (specific to sample collection device), saturation moisture content (3%), moisture content attenuation (2%), burial moisture content (25% relative, unless direct evidence exists of the magnitude and period of differing content), NaI gamma spectrometer calibration (3%) and/or NAA/ICP-MS (2%). Experimental errors are associated with radionuclide quantification for each sample by gamma spectrometry and/or NAA/ICP-MS.

The propagation of these errors through to age calculation is quantified using the expression,

$$\sigma y\ (\delta y/\delta x) = (\Sigma\ ((\delta y/\delta x_n).\sigma x_n)^2)^{1/2} \qquad \text{Eq 2}$$

where y is a value equivalent to that function comprising terms x_n and where σy and σx_n are associated uncertainties.

Errors on age estimates are presented as combined systematic and experimental errors and experimental errors alone. The former (combined) error should be considered when comparing luminescence ages herein with independent chronometric controls. The latter assumes systematic errors are common to luminescence age estimates generated by means equal to those detailed herein and enable direct comparison with those estimates.

8.0 SUMMARY AND RECOMMENDATIONS

The Optical age estimates generated in this study, incorporating analytical uncertainties, span from 31 ka (Marine Isotope Stage 2) to greater than 869 ka (Marine Isotope Stage 24). Though all but one sample, GL10037, are accompanied by a varying range of analytical caveats, within individual cores all age estimates are consistent with their relative stratigraphic position. The antiquity of the oldest age estimates owes itself to some exceptionally low lithogenic D_r values. Whilst below average radionuclide concentrations are conducive to extending the upper age range of optical dating it should be borne in mind that age estimates become increasingly sensitive to inaccuracies in D_r as the magnitude of D_r decreases and burial period increases. The reliability of the optical chronology should be measured against any extrinsic temporal control that may be

available to the project. If units dated in this study can be shown to be stratigraphically equivalent between cores then it may be possible to assess reliability intrinsically, quantifying the convergence of age estimates from divergent D_r values (Toms *et al* 2005).

9.0 REFERENCES

Adamiec, G, and Aitken, M J, 1998 Dose-rate conversion factors: new data, *Ancient TL*, **16**, 37–50

Agersnap Larsen, N, Bulur, E, Bøtter-Jensen, L, and McKeever, S W S, 2000 Use of the LM-OSL technique for the detection of partial bleaching in quartz, *Radiation Measurements*, **32**, 419–25.

Aitken, M J, 1985 *Thermoluminescence dating*, London (Academic Press)

Aitken, M J, 1998 *An Introduction to Optical Dating: the Dating of Quaternary Sediments by the Use of Photon-Stimulated Luminescence*, Oxford (Oxford Univ Press)

Bailey, R M, Singarayer, J S, Ward, S, and Stokes, S, 2003 Identification of partial resetting using D_e as a function of illumination time, *Radiation Measurements*, **37**, 511–18

Banerjee, D, Murray, A S, Bøtter-Jensen, L, and Lang, A, 2001 Equivalent dose estimation using a single aliquot of polymineral fine grains, *Radiation Measurements*, **33**, 73–94

Bateman, M D, Frederick, C D, Jaiswal, M K, and Singhvi, A K, 2003 Investigations into the potential effects of pedoturbation on luminescence dating, *Quaternary Sci Rev*, **22**, 1169–76

Bøtter-Jensen, L, Mejdahl, V, and Murray, A S, 1999 New light on OSL, *Quat Sci Rev*, **18**, 303–10

Bøtter-Jensen, L, McKeever, S W S, and Wintle, A G, 2003 *Optically Stimulated Luminescence Dosimetry*, Amsterdam (Elsevier)

Duller, G A T, 2003 Distinguishing quartz and feldspar in single grain luminescence measurements, *Radiation Measurements*, **37**, 161–5.

Duller, G A T, 2008 *Luminescence Dating: guidelines on using luminescence dating in archaeology.* Swindon (English Heritage)

Galbraith, R F 1990 The radial plot: graphical assessment of spread in ages. *Nuclear Tracks and Radiation Measurements*, **17**, 207–14

Galbraith, R F, Roberts, R G, Laslett, G M, Yoshida, H, and Olley, J M, 1999 Optical dating of single and multiple grains of quartz from Jinmium rock shelter (northern Australia): Part I, Experimental design and statistical models, *Archaeometry*, **41**, 339–64

Hubble, J H, 1982 Photon mass attenuation and energy-absorption coefficients from 1keV to 20MeV, *Int J Applied Radioisotopes*, **33**, 1269–90

Huntley, D J, Godfrey-Smith, D I, and Thewalt, M L W, 1985 Optical dating of sediments, *Nature*, **313**, 105–7

Hütt, G, Jaek, I, and Tchonka, J, 1988 Optical dating: K-feldspars optical response stimulation spectra, *Quaternary Sci Rev*, **7**, 381–6

Jakobsen, M, Backman, J, Murray, A, and Reidar, L, 2003 Optically Stimulated Luminescence dating supports central Arctic Ocean cm-scale sedimentation rates, *Geochem, Geophys, Geosystems*, **4**, 1016

Markey, B G, Bøtter-Jensen, L, and Duller, G A T, 1997 A new flexible system for measuring thermally and optically stimulated luminescence, *Radiation Measurements*, **27**, 83–9

Mejdahl, V, 1979 Thermoluminescence dating: beta-dose attenuation in quartz grains, *Archaeometry*, **21**, 61–72

Murray, A S, and Olley, J M, 2002 Precision and accuracy in the Optically Stimulated Luminescence dating of sedimentary quartz: a status review, *Geochronometria*, **21**, 1–16

Murray, A S and Wintle, A G, 2000 Luminescence dating of quartz using an improved single-aliquot regenerative-dose protocol, *Radiation Measurements*, **32**, 57–73

Murray, A S, and Wintle, A G, 2003 The single aliquot regenerative dose protocol: potential for improvements in reliability. *Radiation Measurements*, **37**, 377–81

Murray, A S, Olley, J M, and Caitcheon, G G, 1995 Measurement of equivalent doses in quartz from contemporary water-lain sediments using optically stimulated luminescence, *Quaternary Sci Rev*, **14**, 365–71

Murray, A S, Wintle, A G, and Wallinga, J, 2002 Dose estimation using quartz OSL in the non-linear region of the growth curve, *Radiation Protection Dosimetry*, **101**, 371–4

Olley, J M, Murray, A S, and Roberts, R G, 1996 The effects of disequilibria in the Uranium and Thorium decay chains on burial dose rates in fluvial sediments. *Quaternary Sci Rev*, **15**, 751–60

Olley, J M, Caitcheon, G G, and Murray, A S, 1998 The distribution of apparent dose as determined by optically stimulated luminescence in small aliquots of fluvial quartz: implications for dating young sediments, *Quat Sci Rev*, **17**, 1033–40

Olley, J M, Caitcheon, G G, and Roberts R G, 1999 The origin of dose distributions in fluvial sediments, and the prospect of dating single grains from fluvial deposits using - optically stimulated luminescence, *Radiation Measurements,* **30,** 207–17

Olley, J M, Pietsch, T, and Roberts, R G, 2004 Optical dating of Holocene sediments from a variety of geomorphic settings using single grains of quartz, *Geomorphol*, **60**, 337–58

Pawley, S M, Toms, P S, Armitage, S J, and Rose, J, 2010 Quartz luminescence dating of Anglian Stage fluvial sediments: Comparison of SAR age estimates to the terrace chronology of the Middle Thames valley, UK, *Quaternary Geochron*, **5**, 569–82

Prescott, J R, and Hutton, J T, 1994 Cosmic ray contributions to dose rates for luminescence and ESR dating: large depths and long-term time variations, *Radiation Measurements*, **23**, 497–500

Smith, B W, Rhodes, E J, Stokes, S, and Spooner, N A, 1990 The optical dating of sediments using quartz, *Radiation Protection Dosimetry*, **34**, 75–8

Spooner, N A, 1993 'The validity of optical dating based on feldspar', unpubl DPhil thesis, Oxford Univ

Stokes, S, Ingram, S, Aitken, M J, Sirocko, F, Anderson, R, and Leuschner, D, 2003 Alternative chronologies for Late Quaternary (Last Interglacial-Holocene) deep sea sediments via optical dating of silt-sized quartz, *Quaternary Sci Rev*, **22**, 925–41

Templer, R H, 1985 The removal of anomalous fading in zircons, *Nuclear Tracks and Radiation Measurements*, **10**, 531–7

Toms, P S, Hosfield, R T, Chambers, J C, Green, C P, and Marshall, P, 2005 Optical dating of the Broom Palaeolithic sites, Devon and Dorset, *EH CfA Rep*, **16/2005**

Wallinga, J, 2002 Optically stimulated luminescence dating of fluvial deposits: a review, *Boreas*, **31**, 303–22

Wintle, A G, 1973 Anomalous fading of thermoluminescence in mineral samples, *Nature*, **245**, 143–4

Zimmerman, D W, 1971 Thermoluminescent dating using fine grains from pottery, *Archaeometry*, **13**, 29–52

TABLES

Field Code	Lab Code	Location	Overburden (m)	Grain size (μm)	Moisture content (%)	Ge γ-spectrometry (external γ field)			γ D_r (Gy.ka^{-1})	Ge γ-spectrometry (external β field)			β D_r (Gy.ka^{-1})	Cosmic D_r (Gy.ka^{-1})	Total D_r (Gy.ka^{-1})	Preheat (°C for 10s)	D_e (Gy)	Age (ka)
						K (%)	Th (ppm)	U (ppm)		K (%)	Th (ppm)	U (ppm)						
VC2b 0.85-0.95 m	GL10038	53°N, 2°E, -28m	0.90	125-180	16 ± 8	-	-	-	0.24 ± 0.05	0.65 ± 0.04	2.04 ± 0.27	0.36 ± 0.05	0.46 ± 0.07	0.18 ± 0.02	0.95 ± 0.11	260	230.1 ± 16.7	243 ± 33 (30)
VC2b 3.10-3.20 m	GL10039	53°N, 2°E, -28m	3.15	125-180	13 ± 7	0.48 ± 0.03	1.84 ± 0.27	0.40 ± 0.06	0.21 ± 0.03	0.51 ± 0.03	1.55 ± 0.27	0.33 ± 0.05	0.38 ± 0.05	0.12 ± 0.01	0.78 ± 0.07	260	326.1 ± 53.4	418 ± 78 (72)
VC3b 5.77-5.87 m	GL10040	53°N, 2°E, -28m	5.82	180-250	15 ± 8	-	-	-	0.18 ± 0.03	0.42 ± 0.03	1.59 ± 0.22	0.32 ± 0.05	0.31 ± 0.05	0.08 ± 0.01	0.63 ± 0.08	280	464.4 ± 64.0	735 ± 134 (125)
VC7b 0.45-0.55 m	GL10041	53°N, 2°E, -27m	0.50	125-180	16 ± 8	0.80 ± 0.04	3.43 ± 0.34	0.87 ± 0.07	0.37 ± 0.05	0.90 ± 0.05	3.54 ± 0.32	0.81 ± 0.07	0.68 ± 0.11	0.19 ± 0.03	1.31 ± 0.12	260	125.3 ± 8.5	96 ± 11 (9)
VC7b 1.32-1.42 m	GL10037	53°N, 2°E, -27m	1.37	125-180	13 ± 7	0.53 ± 0.03	3.63 ± 0.36	0.16 ± 0.05	0.27 ± 0.03	0.61 ± 0.04	1.81 ± 0.28	0.48 ± 0.06	0.47 ± 0.06	0.16 ± 0.02	0.96 ± 0.08	260	105.6 ± 6.2	109 ± 11 (9)
VC7b 2.50-2.65 m	GL10042	53°N, 2°E, -27m	2.57	180-250	8 ± 4	0.13 ± 0.02	0.87 ± 0.07	0.46 ± 0.05	0.12 ± 0.01	0.11 ± 0.02	0.65 ± 0.14	0.44 ± 0.05	0.13 ± 0.02	0.14 ± 0.01	0.45 ± 0.04	240	92.5 ± 6.8	207 ± 24 (18)
VC9b 0.70-0.80 m	GL10045	53°N, 2°E, -27m	0.75	180-250	12 ± 6	0.19 ± 0.02	1.49 ± 0.19	0.30 ± 0.05	0.13 ± 0.02	0.24 ± 0.02	0.89 ± 0.24	0.46 ± 0.05	0.21 ± 0.03	0.18 ± 0.03	0.59 ± 0.05	230	21.2 ± 2.3	36 ± 5 (4)
VC9b 1.45-1.55 m	GL10044	53°N, 2°E, -27m	1.50	125-180	12 ± 6	0.49 ± 0.03	1.67 ± 0.19	0.28 ± 0.05	0.20 ± 0.02	0.59 ± 0.04	1.33 ± 0.15	0.41 ± 0.05	0.44 ± 0.06	0.16 ± 0.02	0.86 ± 0.07	240	31.3 ± 1.5	36 ± 3 (3)
VC9b 4.51-4.61 m	GL10043	53°N, 2°E, -27m	4.56	125-180	15 ± 8	-	-	-	0.32 ± 0.06	0.87 ± 0.01	2.27 ± 0.33	0.58 ± 0.06	0.63 ± 0.10	0.10 ± 0.01	1.11 ± 0.14	220	313.1 ± 47.6	283 ± 56 (53)

Table 1 D_r, D_e and Age data of submitted samples. Uncertainties in age are quoted at 1 σ confidence, are based on analytical errors and reflect combined systematic and experimental variability and (in parentheses) experimental variability alone (see 6.0). Total D_r includes a standard internal α D_r of 0.06 ± 0.03 Gy.ka^{-1}. Blue indicates samples with accepted age estimates; red, age estimates with caveats (see Table 2)

Generic considerations	Field Code	Lab Code	Sample specific considerations
None	VC2b 0.85-0.95 m	GL10038	Overdispersion of regenerative-dose data (see 4.1.4 and Fig 4) Significant U disequilibrium (see 5.0 and Fig 7) Absence of γ field sample (see 5.0) Accept with strong reservations
	VC2b 3.10-3.20 m	GL10039	Overdispersion of regenerative-dose data (see 4.1.4 and Fig 4) Accept tentatively
	VC3b 5.77-5.87 m	GL10040	Overdispersion of regenerative-dose data (see 4.1.4 and Fig 4) Portion (25%) of aliquots saturated (see 4.1.3) Absence of γ field sample (see 5.0) Accept as minimum age estimate
	VC7b 0.45-0.55 m	GL10041	Dose Recovery test failure (see 4.1.2 and Fig 2) Overdispersion of regenerative-dose data (see 4.1.4 and Fig 4) Moderate U disequilibrium (see 5.0 and Fig 7) Accept with strong reservations
	VC7b 1.32-1.42 m	GL10037	Accept
	VC7b 2.50-2.65 m	GL10042	Overdispersion of regenerative-dose data (see 4.1.4 and Fig 4) Possible feldspar contamination (see 4.1.1 and Fig 5) Partially bleached (see 4.2.1 and Fig 6) Accept tentatively
	VC9b 0.70-0.80 m	GL10045	Overdispersion of regenerative-dose data (see 4.1.4 and Fig 4) Accept tentatively
	VC9b 1.45-1.55 m	GL10044	Overdispersion of regenerative-dose data (see 4.1.4 and Fig 4) Accept tentatively
	VC9b 4.51-4.61 m	GL10043	Dose Recovery test failure (see 4.1.2 and Fig 2) Overdispersion of regenerative-dose data (see 4.1.4 and Fig 4) Possible feldspar contamination (see 4.1.1 and Fig 5) Absence of γ field sample (see 5.0) Moderate to significant U disequilibrium (see 5.0 and Fig 7) Accept with strong reservations

Table 2 Analytical validity of sample suite age estimates and caveats for consideration

APPENDIX 1: TECHNICAL DATA FOR SAMPLE GL10038

Fig. 1 Signal Calibration

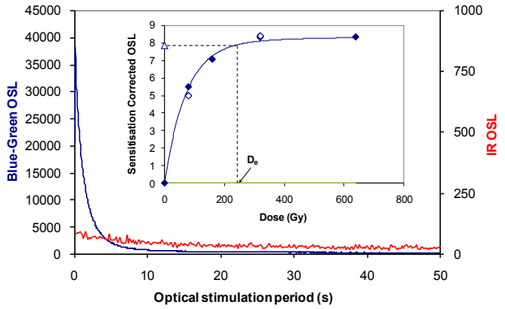

Fig. 1 Signal Calibration Natural blue and laboratory-induced infrared (IR) OSL signals. Detectable IR signal decays are diagnostic of feldspar contamination. Inset, the natural blue OSL signal (open triangle) of each aliquot is calibrated against known laboratoy doses to yield equivalent dose (D_e) values. Repeats of low and high doses (open diamonds) illustate the success of sensitivity correction.

Fig. 2 Dose Recovery The acquisition of D_e values is necessarily predicated upon thermal treatment of aliquots succeeding environmental and laboratoy irradiation. The Dose Recovery test quantifies the combined effects of thermal transfer and sensitisation on the natural signal using a precise lab dose to simulate natural dose. Based on this an appropriate thermal treatment is selected to generate the final D_e value.

Fig. 3 Inter-aliquot D_e distribution Provides a measure of inter-aliquot statistical concordance in D_e values derived from **natural** irradiation. Discordant data (those points lying beyond ±2 standardised ln D_e) reflects heterogeneous dose absorption and/or inaccuracies in calibration.

Fig. 4 Low and High Repeat Regenerative-dose Ratio Measures the statistical concordance of signals from repeated **low** and **high** regenerative-doses. Discordant data (those points lying beyond ±2 standardised ln D_e) indicate inaccurate sensitivity correction.

Fig. 5 OSL to Post-IR OSL Ratio Measures the statistical concordance of OSL and post-IR OSL responses to the same regenerative-dose. Discordant, underestimating data (those points lying below -2 standardised ln D_e) highlight the presence of significant feldspar contamination.

Fig. 6 Signal Analysis Statistically significant increase in **natural** D_e value with signal stimulation period is indicative of a partially-bleached signal, provided a significant increase in D_e results from **simulated partial bleaching** followed by insignificant adjustment in D_e for simulated **zero** and **full bleach** conditions. Ages form such samples are considered maximum estimates. In the absence of a significant rise in D_e with stimulation time, simulated partial bleaching and zero/full bleach tests are not assessed.

Fig. 7 U Activity Statistical concordance (**equilibrium**) in the activities of the daughter radioisotope ^{226}Ra with its parent ^{238}U may signify the temporal stability of D_r emissions from these chains. Significant differences (disequilibrium; **>50%**) in activity indicate addition or removal of isotopes creating a time-dependent shift in D_r values and increased uncertainty in the accuracy of age estimates. A **20%** disequilibrium marker is also shown.

Fig. 8 Age Range The **mean age range** provides an estimate of sediment burial period based on mean D_e and D_r values with associated analytical uncertainties. The **probability distribution** indicates the inter-aliquot variability in age. The **maximum influence** of temporal variations in D_r forced by minima-maxima variation in moisture content and overburden thickness may prove instructive where there is uncertainty in these parametres, however the combined extremes represented should not be construed as preferred age estimates.

Fig. 2 Dose Recovery

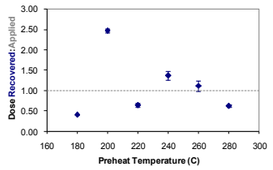

Fig. 3 Inter-aliquot D_e distribution

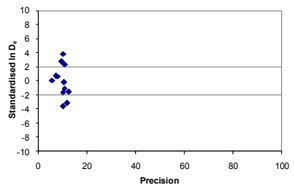

Fig. 4 Low and High Repeat Regenerative-dose Ratio

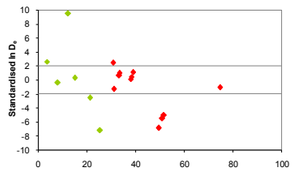

Fig. 5 OSL to Post-IR OSL Ratio

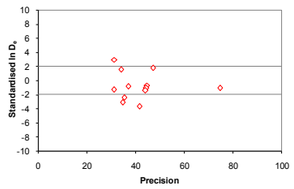

Sample: GL10038

Fig. 6 Signal Analysis

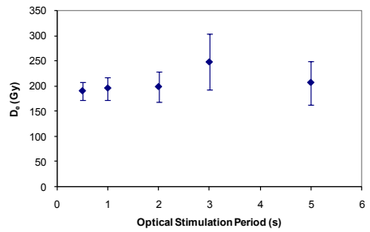

Fig. 7 U Decay Activity

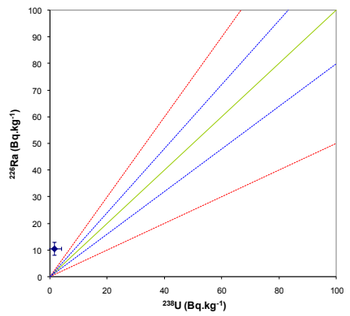

Fig. 8 Age Range

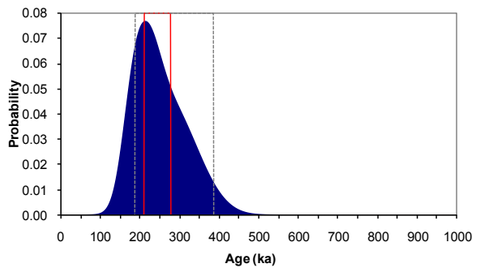

APPENDIX 2: TECHNICAL DATA FOR SAMPLE GL10039

Fig. 1 Signal Calibration

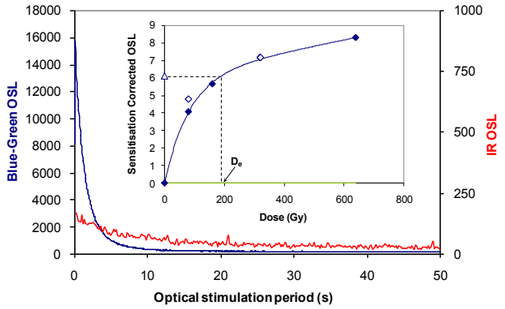

Fig. 1 Signal Calibration Natural blue and laboratory-induced infrared (IR) OSL signals. Detectable IR signal decays are diagnostic of feldspar contamination. Inset, the natural blue OSL signal (open triangle) of each aliquot is calibrated against known laboratory doses to yield equivalent dose (D_e) values. Repeats of low and high doses (open diamonds) illustrate the success of sensitivity correction.

Fig. 2 Dose Recovery The acquisition of D_e values is necessarily predicated upon thermal treatment of aliquots succeeding environmental and laboratory irradiation. The Dose Recovery test quantifies the combined effects of thermal transfer and sensitisation on the natural signal using a precise lab dose to simulate natural dose. Based on this an appropriate thermal treatment is selected to generate the final D_e value.

Fig. 3 Inter-aliquot D_e distribution Provides a measure of inter-aliquot statistical concordance in D_e values derived from **natural** irradiation. Discordant data (those points lying beyond ±2 standardised ln D_e) reflects heterogeneous dose absorption and/or inaccuracies in calibration.

Fig. 4 Low and High Repeat Regenerative-dose Ratio Measures the statistical concordance of signals from repeated **low** and **high** regenerative-doses. Discordant data (those points lying beyond ±2 standardised ln D_e) indicate inaccurate sensitivity correction.

Fig. 5 OSL to Post-IR OSL Ratio Measures the statistical concordance of OSL and post-IR OSL responses to the same regenerative-dose. Discordant, underestimating data (those points lying below -2 standardised ln D_e) highlight the presence of significant feldspar contamination.

Fig. 6 Signal Analysis Statistically significant increase in **natural** D_e value with signal stimulation period is indicative of a partially-bleached signal, provided a significant increase in D_e results from **simulated partial bleaching** followed by insignificant adjustment in D_e for simulated **zero** and **full bleach** conditions. Ages form such samples are considered maximum estimates. In the absence of a significant rise in D_e with stimulation time, simulated partial bleaching and zero/full bleach tests are not assessed.

Fig. 7 U Activity Statistical concordance (**equilibrium**) in the activities of the daughter radioisotope ^{226}Ra with its parent ^{238}U may signify the temporal stability of D_r emissions from these chains. Significant differences (disequilibrium; **>50%**) in activity indicate addition or removal of isotopes creating a time-dependent shift in D_r values and increased uncertainty in the accuracy of age estimates. A **20%** disequilibrium marker is also shown.

Fig. 8 Age Range The **mean age range** provides an estimate of sediment burial period based on mean D_e and D_r values with associated analytical uncertainties. The **probability distribution** indicates the inter-aliquot variability in age. The **maximum influence** of temporal variations in D_r forced by minima-maxima variation in moisture content and overburden thickness may prove instructive where there is uncertainty in these parametres, however the combined extremes represented should not be construed as preferred age estimates.

Fig. 2 Dose Recovery

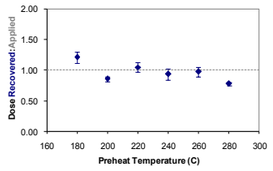

Fig. 3 Inter-aliquot D_e distribution

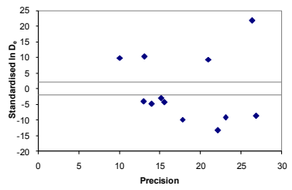

Fig. 4 Low and High Repeat Regenerative-dose Ratio

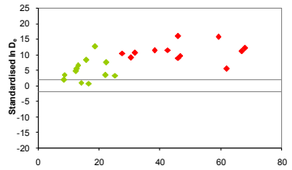

Fig. 5 OSL to Post-IR OSL Ratio

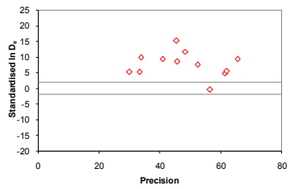

Sample: GL10039

Fig. 6 Signal Analysis

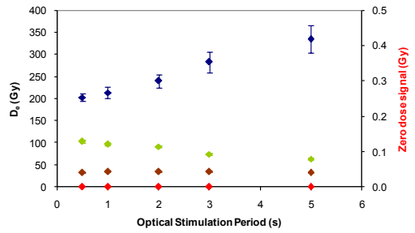

Fig. 7 U Decay Activity

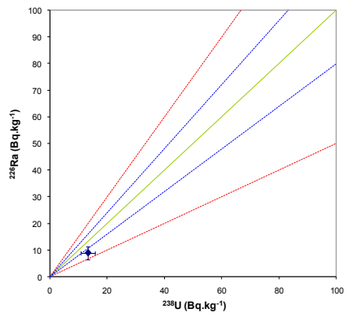

Fig. 8 Age Range

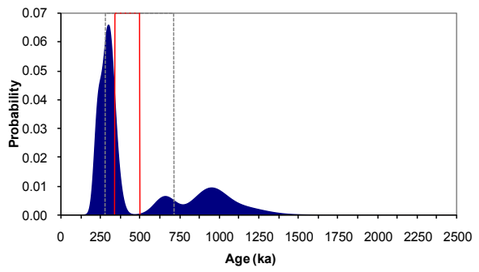

APPENDIX 3: TECHNICAL DATA FOR SAMPLE GL10040

Fig. 1 Signal Calibration

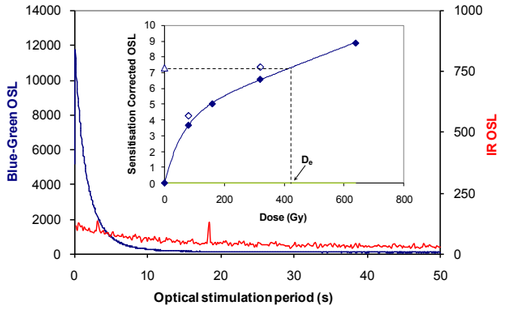

Fig. 1 Signal Calibration Natural blue and laboratory-induced infrared (IR) OSL signals. Detectable IR signal decays are diagnostic of feldspar contamination. Inset, the natural blue OSL signal (open triangle) of each aliquot is calibrated against known laboratoy doses to yield equivalent dose (D_e) values. Repeats of low and high doses (open diamonds) illustate the success of sensitivity correction.

Fig. 2 Dose Recovery The acquisition of D_e values is necessarily predicated upon thermal treatment of aliquots succeeding environmental and laboratoy irradiation. The Dose Recovery test quantifies the combined effects of thermal transfer and sensitisation on the natural signal using a precise lab dose to simulate natural dose. Based on this an appropriate thermal treatment is selected to generate the final D_e value.

Fig. 3 Inter-aliquot D_e distribution Provides a measure of inter-aliquot statistical concordance in D_e values derived from **natural** irradiation. Discordant data (those points lying beyond ±2 standardised ln D_e) reflects heterogeneous dose absorption and/or inaccuracies in calibration.

Fig. 4 Low and High Repeat Regenerative-dose Ratio Measures the statistical concordance of signals from repeated **low** and **high** regenerative-doses. Discordant data (those points lying beyond ±2 standardised ln D_e) indicate inaccurate sensitivity correction.

Fig. 5 OSL to Post-IR OSL Ratio Measures the statistical concordance of OSL and post-IR OSL responses to the same regenerative-dose. Discordant, underestimating data (those points lying below -2 standardised ln D_e) highlight the presence of significant feldspar contamination.

Fig. 6 Signal Analysis Statistically significant increase in **natural** D_e value with signal stimulation period is indicative of a partially-bleached signal, provided a significant increase in D_e results from **simulated partial bleaching** followed by insignificant adjustment in D_e for simulated **zero** and **full bleach** conditions. Ages form such samples are considered maximum estimates. In the absence of a significant rise in D_e with stimulation time, simulated partial bleaching and zero/full bleach tests are not assessed.

Fig. 7 U Activity Statistical concordance (**equilibrium**) in the activities of the daughter radioisotope ^{226}Ra with its parent ^{238}U may signify the temporal stability of D_r emissions from these chains. Significant differences (disequilibrium; **>50%**) in activity indicate addition or removal of isotopes creating a time-dependent shift in D_r values and increased uncertainty in the accuracy of age estimates. A **20%** disequilibrium marker is also shown.

Fig. 8 Age Range The **mean age range** provides an estimate of sediment burial period based on mean D_e and D_r values with associated analytical uncertainties. The **probability distribution** indicates the inter-aliquot variability in age. The **maximum influence** of temporal variations in D_r forced by minima-maxima variation in moisture content and overburden thickness may prove instructive where there is uncertainty in these parametres, however the combined extremes represented should not be construed as preferred age estimates.

Fig. 2 Dose Recovery

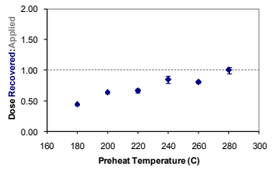

Fig. 3 Inter-aliquot D_e distribution

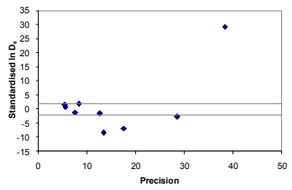

Fig. 4 Low and High Repeat Regenerative-dose Ratio

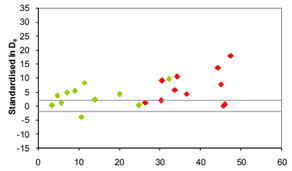

Fig. 5 OSL to Post-IR OSL Ratio

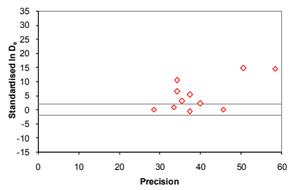

Sample: GL10040

Fig. 6 Signal Analysis

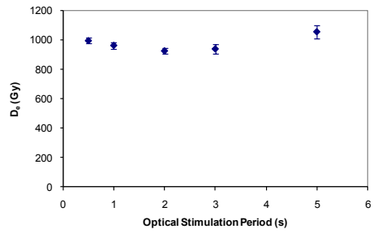

Fig. 7 U Decay Activity

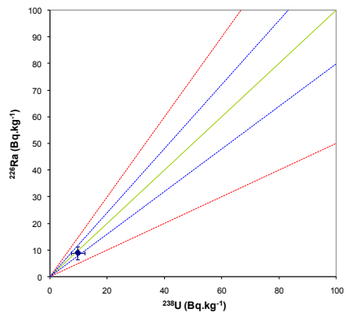

Fig. 8 Age Range

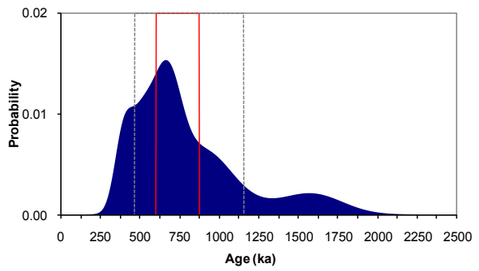

APPENDIX 4: TECHNICAL DATA FOR SAMPLE GL10041

Fig. 1 Signal Calibration

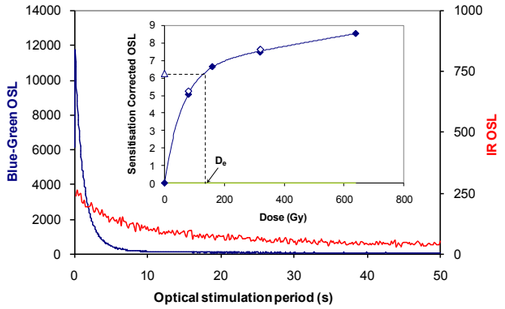

Fig. 1 Signal Calibration Natural blue and laboratory-induced infrared (IR) OSL signals. Detectable IR signal decays are diagnostic of feldspar contamination. Inset, the natural blue OSL signal (open triangle) of each aliquot is calibrated against known laboratory doses to yield equivalent dose (D_e) values. Repeats of low and high doses (open diamonds) illustrate the success of sensitivity correction.

Fig. 2 Dose Recovery The acquisition of D_e values is necessarily predicated upon thermal treatment of aliquots succeeding environmental and laboratory irradiation. The Dose Recovery test quantifies the combined effects of thermal transfer and sensitisation on the natural signal using a precise lab dose to simulate natural dose. Based on this an appropriate thermal treatment is selected to generate the final D_e value.

Fig. 3 Inter-aliquot D_e distribution Provides a measure of inter-aliquot statistical concordance in D_e values derived from **natural** irradiation. Discordant data (those points lying beyond ±2 standardised ln D_e) reflects heterogeneous dose absorption and/or inaccuracies in calibration.

Fig. 4 Low and High Repeat Regenerative-dose Ratio Measures the statistical concordance of signals from repeated **low** and **high** regenerative-doses. Discordant data (those points lying beyond ±2 standardised ln D_e) indicate inaccurate sensitivity correction.

Fig. 5 OSL to Post-IR OSL Ratio Measures the statistical concordance of OSL and post-IR OSL responses to the same regenerative-dose. Discordant, underestimating data (those points lying below -2 standardised ln D_e) highlight the presence of significant feldspar contamination.

Fig. 6 Signal Analysis Statistically significant increase in **natural** D_e value with signal stimulation period is indicative of a partially-bleached signal, provided a significant increase in D_e results from **simulated partial bleaching** followed by insignificant adjustment in D_e for simulated **zero** and **full bleach** conditions. Ages form such samples are considered maximum estimates. In the absence of a significant rise in D_e with stimulation time, simulated partial bleaching and zero/full bleach tests are not assessed.

Fig. 7 U Activity Statistical concordance (**equilibrium**) in the activities of the daughter radioisotope ^{226}Ra with its parent ^{238}U may signify the temporal stability of D_r emissions from these chains. Significant differences (disequilibrium; **>50%**) in activity indicate addition or removal of isotopes creating a time-dependent shift in D_r values and increased uncertainty in the accuracy of age estimates. A **20%** disequilibrium marker is also shown.

Fig. 8 Age Range The **mean age range** provides an estimate of sediment burial period based on mean D_e and D_r values with associated analytical uncertainties. The **probability distribution** indicates the inter-aliquot variability in age. The **maximum influence** of temporal variations in D_r forced by minima-maxima variation in moisture content and overburden thickness may prove instructive where there is uncertainty in these parametres, however the combined extremes represented should not be construed as preferred age estimates.

Fig. 2 Dose Recovery

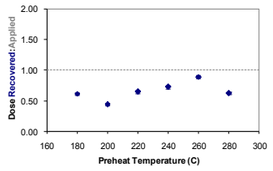

Fig. 3 Inter-aliquot D_e distribution

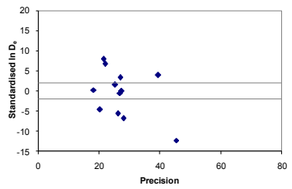

Fig. 4 Low and High Repeat Regenerative-dose Ratio

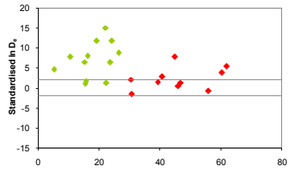

Fig. 5 OSL to Post-IR OSL Ratio

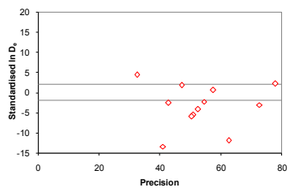

Sample: GL10041

Fig. 6 Signal Analysis

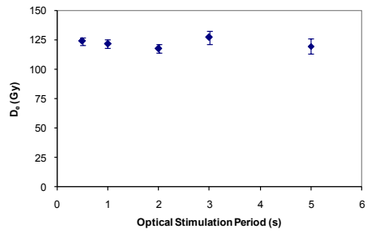

Fig. 7 U Decay Activity

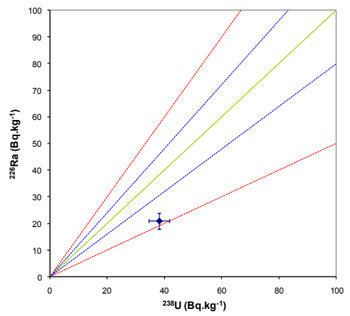

Fig. 8 Age Range

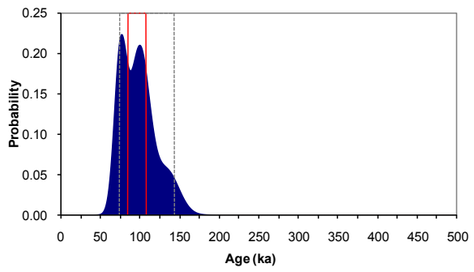

APPENDIX 5: TECHNICAL DATA FOR SAMPLE GL10037

Fig. 1 Signal Calibration

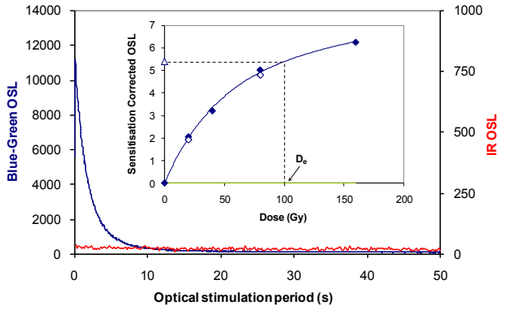

Fig. 1 Signal Calibration Natural blue and laboratory-induced infrared (IR) OSL signals. Detectable IR signal decays are diagnostic of feldspar contamination. Inset, the natural blue OSL signal (open triangle) of each aliquot is calibrated against known laboratoy doses to yield equivalent dose (D_e) values. Repeats of low and high doses (open diamonds) illustate the success of sensitivity correction.

Fig. 2 Dose Recovery The acquisition of D_e values is necessarily predicated upon thermal treatment of aliquots succeeding environmental and laboratory irradiation. The Dose Recovery test quantifies the combined effects of thermal transfer and sensitisation on the natural signal using a precise lab dose to simulate natural dose. Based on this an appropriate thermal treatment is selected to generate the final D_e value.

Fig. 3 Inter-aliquot D_e distribution Provides a measure of inter-aliquot statistical concordance in D_e values derived from **natural** irradiation. Discordant data (those points lying beyond ±2 standardised ln D_e) reflects heterogeneous dose absorption and/or inaccuracies in calibration.

Fig. 4 Low and High Repeat Regenerative-dose Ratio Measures the statistical concordance of signals from repeated **low** and **high** regenerative-doses. Discordant data (those points lying beyond ±2 standardised ln D_e) indicate inaccurate sensitivity correction.

Fig. 5 OSL to Post-IR OSL Ratio Measures the statistical concordance of OSL and post-IR OSL responses to the same regenerative-dose. Discordant, underestimating data (those points lying below -2 standardised ln D_e) highlight the presence of significant feldspar contamination.

Fig. 6 Signal Analysis Statistically significant increase in **natural** D_e value with signal stimulation period is indicative of a partially-bleached signal, provided a significant increase in D_e results from **simulated partial bleaching** followed by insignificant adjustment in D_e for simulated **zero** and **full bleach** conditions. Ages form such samples are considered maximum estimates. In the absence of a significant rise in D_e with stimulation time, simulated partial bleaching and zero/full bleach tests are not assessed.

Fig. 7 U Activity Statistical concordance (**equilibrium**) in the activities of the daughter radioisotope ^{226}Ra with its parent ^{238}U may signify the temporal stability of D_r emissions from these chains. Significant differences (disequilibrium; **>50%**) in activity indicate addition or removal of isotopes creating a time-dependent shift in D_r values and increased uncertainty in the accuracy of age estimates. A **20%** disequilibrium marker is also shown.

Fig. 8 Age Range The **mean age range** provides an estimate of sediment burial period based on mean D_e and D_r values with associated analytical uncertainties. The **probability distribution** indicates the inter-aliquot variability in age. The **maximum influence** of temporal variations in D_r forced by minima-maxima variation in moisture content and overburden thickness may prove instructive where there is uncertainty in these parametres, however the combined extremes represented should not be construed as preferred age estimates.

Fig. 2 Dose Recovery

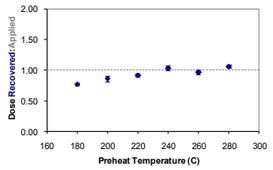

Fig. 3 Inter-aliquot D_e distribution

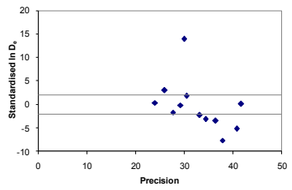

Fig. 4 Low and High Repeat Regenerative-dose Ratio

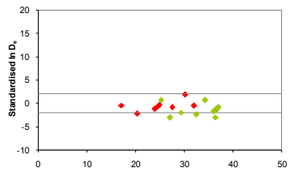

Fig. 5 OSL to Post-IR OSL Ratio

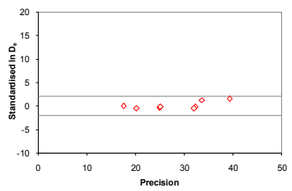

Sample: GL10037

Fig. 6 Signal Analysis

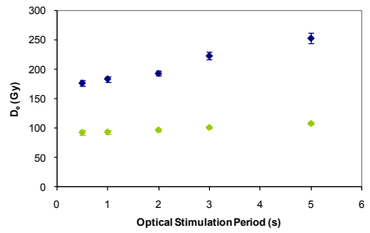

Fig. 7 U Decay Activity

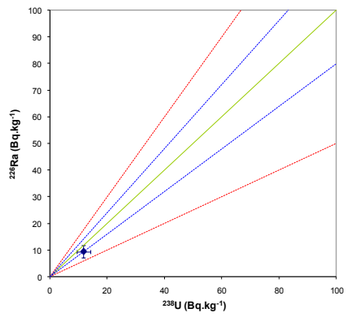

Fig. 8 Age Range

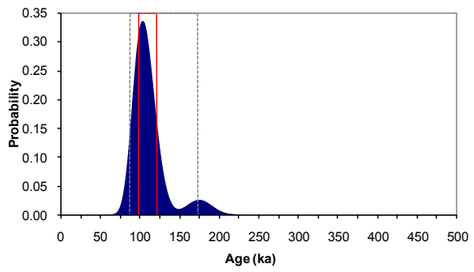

APPENDIX 6: TECHNICAL DATA FOR SAMPLE GL10042

Fig. 1 Signal Calibration

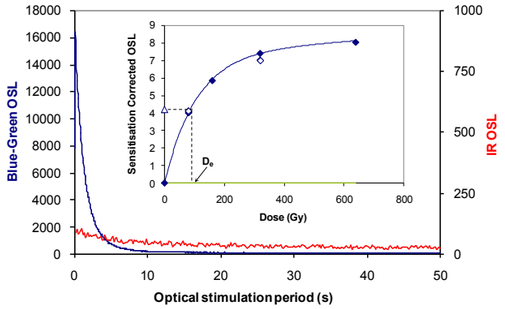

Fig. 1 Signal Calibration Natural blue and laboratory-induced infrared (IR) OSL signals. Detectable IR signal decays are diagnostic of feldspar contamination. Inset, the natural blue OSL signal (open triangle) of each aliquot is calibrated against known laboratoy doses to yield equivalent dose (D_e) values. Repeats of low and high doses (open diamonds) illustate the success of sensitivity correction.

Fig. 2 Dose Recovery The acquisition of D_e values is necessarily predicated upon thermal treatment of aliquots succeeding environmental and laboratoy irradiation. The Dose Recovery test quantifies the combined effects of thermal transfer and sensitisation on the natural signal using a precise lab dose to simulate natural dose. Based on this an appropriate thermal treatment is selected to generate the final D_e value.

Fig. 3 Inter-aliquot D_e distribution Provides a measure of inter-aliquot statistical concordance in D_e values derived from **natural** irradiation. Discordant data (those points lying beyond ±2 standardised ln D_e) reflects heterogeneous dose absorption and/or inaccuracies in calibration.

Fig. 4 Low and High Repeat Regenerative-dose Ratio Measures the statistical concordance of signals from repeated **low** and **high** regenerative-doses. Discordant data (those points lying beyond ±2 standardised ln D_e) indicate inaccurate sensitivity correction.

Fig. 5 OSL to Post-IR OSL Ratio Measures the statistical concordance of OSL and post-IR OSL responses to the same regenerative-dose. Discordant, underestimating data (those points lying below -2 standardised ln D_e) highlight the presence of significant feldspar contamination.

Fig. 6 Signal Analysis Statistically significant increase in **natural** D_e value with signal stimulation period is indicative of a partially-bleached signal, provided a significant increase in D_e results from **simulated partial bleaching** followed by insignificant adjustment in D_e for simulated **zero** and **full bleach** conditions. Ages form such samples are considered maximum estimates. In the absence of a significant rise in D_e with stimulation time, simulated partial bleaching and zero/full bleach tests are not assessed.

Fig. 7 U Activity Statistical concordance (**equilibrium**) in the activities of the daughter radioisotope ^{226}Ra with its parent ^{238}U may signify the temporal stability of D_r emissions from these chains. Significant differences (disequilibrium; **>50%**) in activity indicate addition or removal of isotopes creating a time-dependent shift in D_r values and increased uncertainty in the accuracy of age estimates. A **20%** disequilibrium marker is also shown.

Fig. 8 Age Range The **mean age range** provides an estimate of sediment burial period based on mean D_e and D_r values with associated analytical uncertainties. The **probability distribution** indicates the inter-aliquot variability in age. The **maximum influence** of temporal variations in D_r forced by minima-maxima variation in moisture content and overburden thickness may prove instructive where there is uncertainty in these parametes, however the combined extremes represented should not be construed as preferred age estimates.

Fig. 2 Dose Recovery

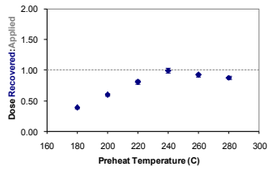

Fig. 3 Inter-aliquot D_e distribution

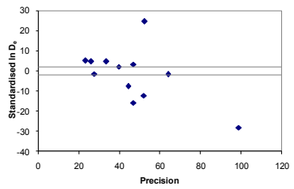

Fig. 4 Low and High Repeat Regenerative-dose Ratio

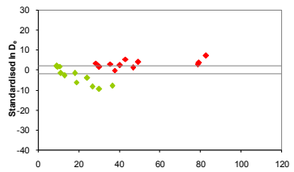

Fig. 5 OSL to Post-IR OSL Ratio

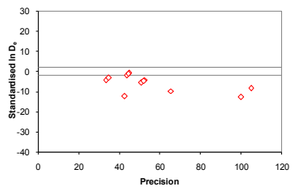

Sample: GL10042

Fig. 6 Signal Analysis

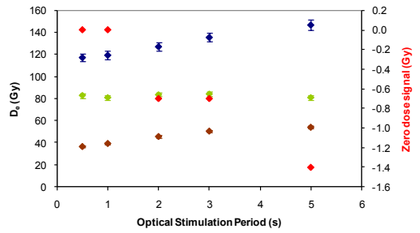

Fig. 7 U Decay Activity

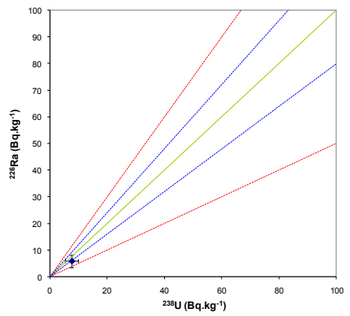

Fig. 8 Age Range

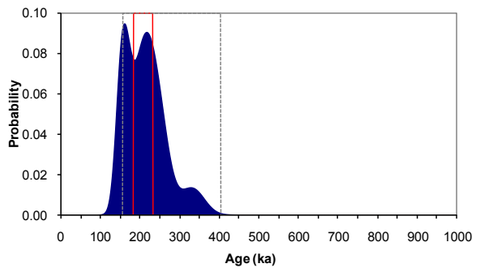

APPENDIX 7: TECHNICAL DATA FOR SAMPLE GL10045

Fig. 1 Signal Calibration

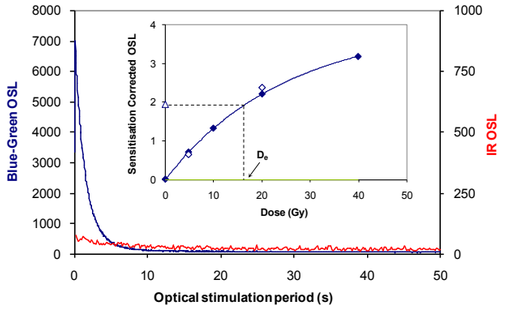

Fig. 1 Signal Calibration Natural blue and laboratory-induced infrared (IR) OSL signals. Detectable IR signal decays are diagnostic of feldspar contamination. Inset, the natural blue OSL signal (open triangle) of each aliquot is calibrated against known laboratory doses to yield equivalent dose (D_e) values. Repeats of low and high doses (open diamonds) illustrate the success of sensitivity correction.

Fig. 2 Dose Recovery The acquisition of D_e values is necessarily predicated upon thermal treatment of aliquots succeeding environmental and laboratory irradiation. The Dose Recovery test quantifies the combined effects of thermal transfer and sensitisation on the natural signal using a precise lab dose to simulate natural dose. Based on this an appropriate thermal treatment is selected to generate the final D_e value.

Fig. 3 Inter-aliquot D_e distribution Provides a measure of inter-aliquot statistical concordance in D_e values derived from **natural** irradiation. Discordant data (those points lying beyond ±2 standardised ln D_e) reflects heterogeneous dose absorption and/or inaccuracies in calibration.

Fig. 4 Low and High Repeat Regenerative-dose Ratio Measures the statistical concordance of signals from repeated **low** and **high** regenerative-doses. Discordant data (those points lying beyond ±2 standardised ln D_e) indicate inaccurate sensitivity correction.

Fig. 5 OSL to Post-IR OSL Ratio Measures the statistical concordance of OSL and post-IR OSL responses to the same regenerative-dose. Discordant, underestimating data (those points lying below -2 standardised ln D_e) highlight the presence of significant feldspar contamination.

Fig. 6 Signal Analysis Statistically significant increase in **natural** D_e value with signal stimulation period is indicative of a partially-bleached signal, provided a significant increase in D_e results from **simulated partial bleaching** followed by insignificant adjustment in D_e for simulated **zero** and **full bleach** conditions. Ages form such samples are considered maximum estimates. In the absence of a significant rise in D_e with stimulation time, simulated partial bleaching and zero/full bleach tests are not assessed.

Fig. 7 U Activity Statistical concordance (**equilibrium**) in the activities of the daughter radioisotope ^{226}Ra with its parent ^{238}U may signify the temporal stability of D_r emissions from these chains. Significant differences (disequilibrium; **>50%**) in activity indicate addition or removal of isotopes creating a time-dependent shift in D_r values and increased uncertainty in the accuracy of age estimates. A **20%** disequilibrium marker is also shown.

Fig. 8 Age Range The **mean age range** provides an estimate of sediment burial period based on mean D_e and D_r values with associated analytical uncertainties. The **probability distribution** indicates the inter-aliquot variability in age. The **maximum influence** of temporal variations in D_r forced by minima-maxima variation in moisture content and overburden thickness may prove instructive where there is uncertainty in these parametres, however the combined extremes represented should not be construed as preferred age estimates.

Fig. 2 Dose Recovery

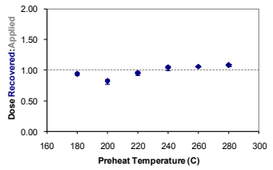

Fig. 3 Inter-aliquot D_e distribution

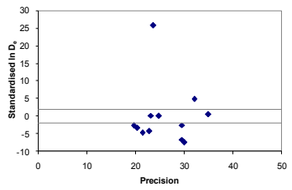

Fig. 4 Low and High Repeat Regenerative-dose Ratio

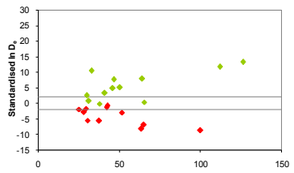

Fig. 5 OSL to Post-IR OSL Ratio

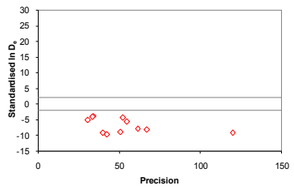

Sample: GL10045

Fig. 6 Signal Analysis

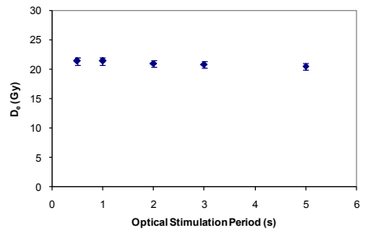

Fig. 7 U Decay Activity

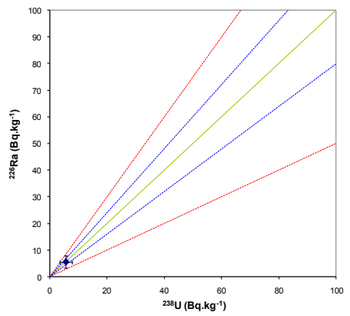

Fig. 8 Age Range

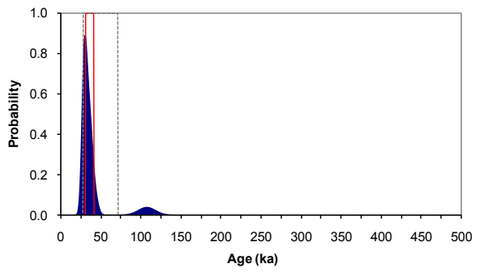

APPENDIX 8: TECHNICAL DATA FOR SAMPLE GL10044

Fig. 1 Signal Calibration

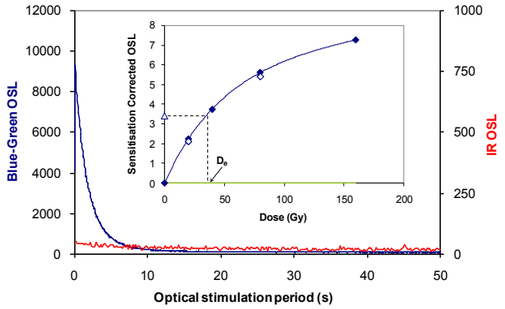

Fig. 1 Signal Calibration Natural blue and laboratory-induced infrared (IR) OSL signals. Detectable IR signal decays are diagnostic of feldspar contamination. Inset, the natural blue OSL signal (open triangle) of each aliquot is calibrated against known laboratory doses to yield equivalent dose (D_e) values. Repeats of low and high doses (open diamonds) illustrate the success of sensitivity correction.

Fig. 2 Dose Recovery The acquisition of D_e values is necessarily predicated upon thermal treatment of aliquots succeeding environmental and laboratory irradiation. The Dose Recovery test quantifies the combined effects of thermal transfer and sensitisation on the natural signal using a precise lab dose to simulate natural dose. Based on this an appropriate thermal treatment is selected to generate the final D_e value.

Fig. 3 Inter-aliquot D_e distribution Provides a measure of inter-aliquot statistical concordance in D_e values derived from **natural** irradiation. Discordant data (those points lying beyond **±2 standardised ln D_e**) reflects heterogeneous dose absorption and/or inaccuracies in calibration.

Fig. 4 Low and High Repeat Regenerative-dose Ratio Measures the statistical concordance of signals from repeated **low** and **high** regenerative-doses. Discordant data (those points lying beyond **±2 standardised ln D_e**) indicate inaccurate sensitivity correction.

Fig. 5 OSL to Post-IR OSL Ratio Measures the statistical concordance of OSL and post-IR OSL responses to the same regenerative-dose. Discordant, underestimating data (those points lying below **-2 standardised ln D_e**) highlight the presence of significant feldspar contamination.

Fig. 6 Signal Analysis Statistically significant increase in **natural** D_e value with signal stimulation period is indicative of a partially-bleached signal, provided a significant increase in D_e results from **simulated partial bleaching** followed by insignificant adjustment in D_e for simulated **zero** and **full bleach** conditions. Ages from such samples are considered maximum estimates. In the absence of a significant rise in D_e with stimulation time, simulated partial bleaching and zero/full bleach tests are not assessed.

Fig. 7 U Activity Statistical concordance (**equilibrium**) in the activities of the daughter radioisotope ^{226}Ra with its parent ^{238}U may signify the temporal stability of D_r emissions from these chains. Significant differences (disequilibrium; **>50%**) in activity indicate addition or removal of isotopes creating a time-dependent shift in D_r values and increased uncertainty in the accuracy of age estimates. A **20%** disequilibrium marker is also shown.

Fig. 8 Age Range The **mean age range** provides an estimate of sediment burial period based on mean D_e and D_r values with associated analytical uncertainties. The **probability distribution** indicates the inter-aliquot variability in age. The **maximum influence** of temporal variations in D_r forced by minima-maxima variation in moisture content and overburden thickness may prove instructive where there is uncertainty in these parametres, however the combined extremes represented should not be construed as preferred age estimates.

Fig. 2 Dose Recovery

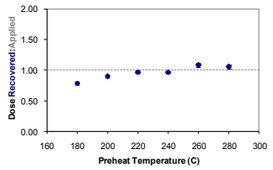

Fig. 3 Inter-aliquot D_e distribution

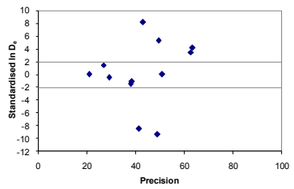

Fig. 4 Low and High Repeat Regenerative-dose Ratio

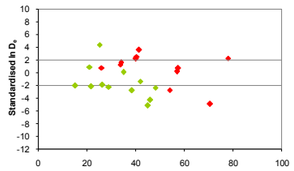

Fig. 5 OSL to Post-IR OSL Ratio

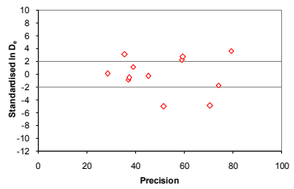

Sample: GL10044

Fig. 6 Signal Analysis

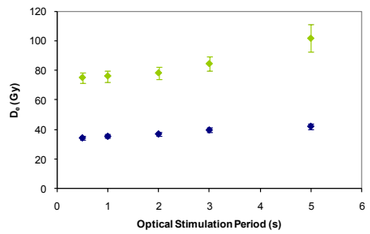

Fig. 7 U Decay Activity

^{226}Ra activity beneath detection limits

Fig. 8 Age Range

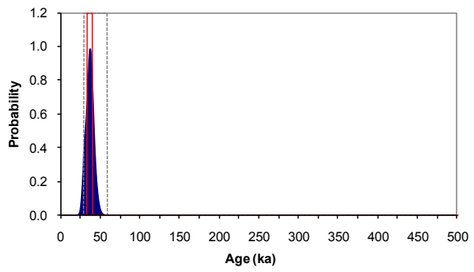

APPENDIX 9: TECHNICAL DATA FOR SAMPLE GL10043

Fig. 1 Signal Calibration

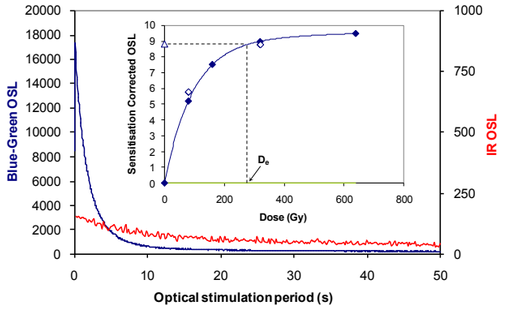

Fig. 1 Signal Calibration Natural blue and laboratory-induced infrared (IR) OSL signals. Detectable IR signal decays are diagnostic of feldspar contamination. Inset, the natural blue OSL signal (open triangle) of each aliquot is calibrated against known laboratoy doses to yield equivalent dose (D_e) values. Repeats of low and high doses (open diamonds) illustate the success of sensitivity correction.

Fig. 2 Dose Recovery The acquisition of D_e values is necessarily predicated upon thermal treatment of aliquots succeeding environmental and laboratory irradiation. The Dose Recovery test quantifies the combined effects of thermal transfer and sensitisation on the natural signal using a precise lab dose to simulate natural dose. Based on this an appropriate thermal treatment is selected to generate the final D_e value.

Fig. 3 Inter-aliquot D_e distribution Provides a measure of inter-aliquot statistical concordance in D_e values derived from **natural** irradiation. Discordant data (those points lying beyond ±2 standardised ln D_e) reflects heterogeneous dose absorption and/or inaccuracies in calibration.

Fig. 4 Low and High Repeat Regenerative-dose Ratio Measures the statistical concordance of signals from repeated **low** and **high** regenerative-doses. Discordant data (those points lying beyond ±2 standardised ln D_e) indicate inaccurate sensitivity correction.

Fig. 5 OSL to Post-IR OSL Ratio Measures the statistical concordance of OSL and post-IR OSL responses to the same regenerative-dose. Discordant, underestimating data (those points lying below -2 standardised ln D_e) highlight the presence of significant feldspar contamination.

Fig. 6 Signal Analysis Statistically significant increase in **natural** D_e value with signal stimulation period is indicative of a partially-bleached signal, provided a significant increase in D_e results from **simulated partial bleaching** followed by insignificant adjustment in D_e for simulated **zero** and **full bleach** conditions. Ages form such samples are considered maximum estimates. In the absence of a significant rise in D_e with stimulation time, simulated partial bleaching and zero/full bleach tests are not assessed.

Fig. 7 U Activity Statistical concordance (**equilibrium**) in the activities of the daughter radioisotope ^{226}Ra with its parent ^{238}U may signify the temporal stability of D, emissions from these chains. Significant differences (disequilibrium; **>50%**) in activity indicate addition or removal of isotopes creating a time-dependent shift in D, values and increased uncertainty in the accuracy of age estimates. A **20%** disequilibrium marker is also shown.

Fig. 8 Age Range The **mean age range** provides an estimate of sediment burial period based on mean D_e and D, values with associated analytical uncertainties. The **probability distribution** indicates the inter-aliquot variability in age. The **maximum influence** of temporal variations in D, forced by minima-maxima variation in moisture content and overburden thickness may prove instructive where there is uncertainty in these parametres, however the combined extremes represented should not be construed as preferred age estimates.

Fig. 2 Dose Recovery

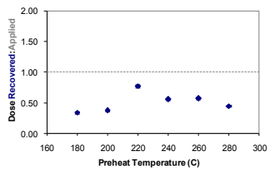

Fig. 3 Inter-aliquot D_e distribution

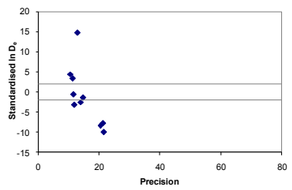

Fig. 4 Low and High Repeat Regenerative-dose Ratio

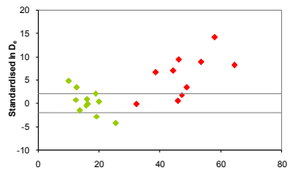

Fig. 5 OSL to Post-IR OSL Ratio

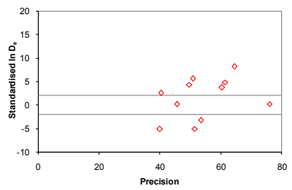

Sample: GL10043

Fig. 6 Signal Analysis

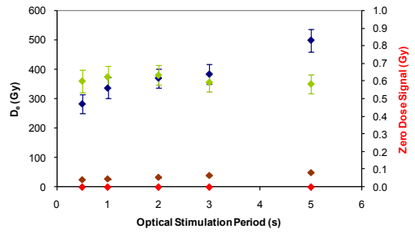

Fig. 7 U Decay Activity

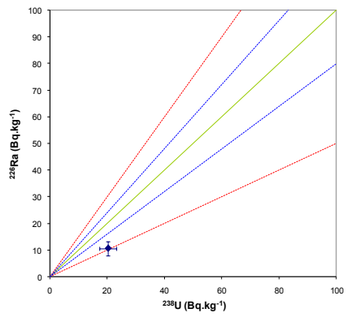

Fig. 8 Age Range

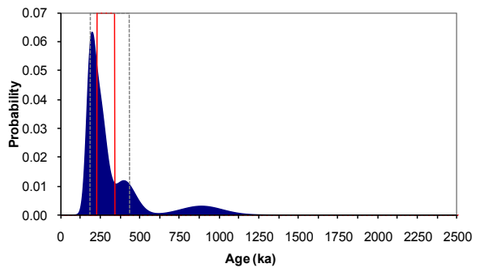

ENGLISH HERITAGE RESEARCH DEPARTMENT

English Heritage undertakes and commissions research into the historic environment, and the issues that affect its condition and survival, in order to provide the understanding necessary for informed policy and decision making, for sustainable management, and to promote the widest access, appreciation and enjoyment of our heritage.

The Research Department provides English Heritage with this capacity in the fields of buildings history, archaeology, and landscape history. It brings together seven teams with complementary investigative and analytical skills to provide integrated research expertise across the range of the historic environment. These are:

* *Aerial Survey and Investigation*
* *Archaeological Projects (excavation)*
* *Archaeological Science*
* *Archaeological Survey and Investigation (landscape analysis)*
* *Architectural Investigation*
* *Imaging, Graphics and Survey (including measured and metric survey, and photography)*
* *Survey of London*

The Research Department undertakes a wide range of investigative and analytical projects, and provides quality assurance and management support for externally-commissioned research. We aim for innovative work of the highest quality which will set agendas and standards for the historic environment sector. In support of this, and to build capacity and promote best practice in the sector, we also publish guidance and provide advice and training. We support outreach and education activities and build these in to our projects and programmes wherever possible.

We make the results of our work available through the Research Department Report Series, and through journal publications and monographs. Our publication Research News, which appears three times a year, aims to keep our partners within and outside English Heritage up-to-date with our projects and activities. A full list of Research Department Reports, with abstracts and information on how to obtain copies, may be found on www.english-heritage.org.uk/researchreports

For further information visit www.english-heritage.org.uk

ENGLISH HERITAGE